

~~CONFIDENTIAL~~C 2 6
Copy
RM E51H27

NACA RM E51H27

UNAVAILABLE

NACA

RESEARCH MEMORANDUM

PRESSURE RECOVERY, DRAG, AND SUBCRITICAL STABILITY

CHARACTERISTICS OF THREE CONICAL SUPERSONIC

DIFFUSERS AT STREAM MACH NUMBERS

FROM 1.7 TO 2.0

By Theodore J. Nussdorfer, Leonard J. Obery
and Gerald W. Englert

Lewis Flight Propulsion Laboratory

CLASSIFICATION ~~CONFIDENTIAL~~
Cleveland, Ohio
UNAVAILABLE

To: UNCLASSIFIED

By authority of

NACA Pro Abs
FRN-119

Effective

Aug. 16, 1957

MMT 9-3-57

CLASSIFIED DOCUMENT

This material contains information affecting the National Defense of the United States within the meaning of the espionage laws, Title 18, U.S.C., Secs. 793 and 794, the transmission or revelation of which in any manner to unauthorized person is prohibited by law.

NATIONAL ADVISORY COMMITTEE
FOR AERONAUTICS

WASHINGTON

February 27, 1952

~~CONFIDENTIAL~~



NATIONAL ADVISORY COMMITTEE FOR AERONAUTICS

RESEARCH MEMORANDUM

PRESSURE RECOVERY, DRAG, AND SUBCRITICAL STABILITY

CHARACTERISTICS OF THREE CONICAL SUPERSONIC

DIFFUSERS AT STREAM MACH NUMBERS FROM 1.7 TO 2.0

By Theodore J. Nussdorfer, Leonard J. Obery
and Gerald W. Englert

SUMMARY

A study of a 20° and a 25° half-angle low mass-flow ratio and a 25° half-angle high mass-flow ratio conical supersonic inlet was made on a 16-inch ram jet in the 8- by 6-foot supersonic tunnel. A greater range of stable subcritical operation was obtained with the low mass-flow ratio inlets; a greater range was obtained with the 25° than with the 20° half-angle low mass-flow ratio inlet. The high mass-flow ratio inlet had the lowest drag.

INTRODUCTION

If the flight schedule of a supersonic vehicle includes acceleration, climbing, or maneuvering, air-flow regulation is required. Many types of supersonic inlet exhibit a severe pulsing condition and concomitant reductions in pressure recovery when the air flow is reduced much below the maximum value. A greater stable range of air flow is obtained with annular inlets having conical center bodies when the cone angle is increased or the stream Mach number decreased, causing the oblique shock generated by the cone to fall outside the cowl lip (references 1 and 2). However, as air is spilled around the cowl, there is an increase in drag (reference 3). The selection of a supersonic inlet therefore often becomes a compromise between the amount of stable air-flow regulation desired and the drag increase that can be tolerated.

In order to provide some insight into the drag penalties resulting from operating an inlet at a stream Mach number considerably below design value, an investigation of a ram-jet engine designed for Project Rigel was conducted in the 8- by 6-foot supersonic tunnel of the NACA Lewis laboratory.

Three inlets designed for use at stream Mach numbers from 1.7 to 2.0 were studied: 20° and 25° half-angle cones having cowls positioned for zero additive drag at a stream Mach number of 3.6, and a 25° half-angle cone inlet designed for zero additive drag at a Mach number of 2.0. The two inlets designed for Mach number 3.6 are designated low mass-flow ratio inlets and that designed for M_0 of 2.0, a high mass-flow ratio inlet.

This report presents the cold-flow diffuser pressure recoveries and the drag characteristics of the three inlets considered at zero angle of attack and over a range of free-stream Mach number from 1.7 to 2.0. The Reynolds number, based on stream conditions and the cowl inlet diameter, was $3.5-5.0 \times 10^6$.

APPARATUS AND PROCEDURE

A schematic diagram of the engine installation is shown in figure 1. The model was supported by a swept-back vertical strut attached to the tunnel balance system. An auxiliary strut, not connected to the tunnel balance system, supported a movable plug at the engine exit. The engine was 15.5 feet long, of which, for reasons dictated by tactical storage requirements, approximately 10 feet was diffuser. (See table I for the coordinates.) Four longerons, two vertical and two horizontal, extended from station 2 to station 3 (fig. 1). Inlet changes were made forward of the position indicated on the figure.

The inlets studied had no internal contraction. They are shown schematically in figure 2 and their coordinates are given in table II. For convenience in identification the diffusers are referred to by a double number system. The first number of the designation is the cone half-angle, the second number is the cowl position half-angle (see fig. 2). For the Mach number range covered in this investigation, approximately the same maximum stream tube of air entered each inlet. Moreover, the diffuser-area ratio was so designed that the critical combustion-chamber-inlet Mach number was approximately the same for all three inlets.

Total- and static-pressure survey stations were located at stations 1 and 3. A survey of static pressures was taken at station 4. Internal static wall orifices were placed on the center body and outer shell as well as on the nozzle. External static wall orifices were located

on the cowl and the boattail. For one run a total-pressure survey of the external boundary layer was made at station 5. Fluctuations in static pressure at station 3 were obtained with a commercial differential-pressure pickup.

The movable plug at the nozzle exit was used to vary the mass flow through the diffuser. Mass-flow computations were based on static-pressure measurements at station 4 and the choked exit area established by the movable plug. In addition, the mass flow was also computed from pressure-rake data obtained in the diffuser and theoretical values were determined from conical-flow theory. The agreement of these three methods of calculation indicate that the absolute value of mass flow is accurate to within 3 percent.

A dummy strut was employed in separating the support strut drag from the forces on the engine body (see reference 4). The external body drags presented do not include the boattail drag of the exit nozzle and represent the external drag with a constant-area combustion chamber.

SYMBOLS

The following symbols are used in this report:

A	area (sq ft)
a/a_a	ratio of local to stagnation speed of sound
B	$\sqrt{M^2-1}$
C_D	external-body-drag coefficient, $D/q_0 A_{max}$
C_p	pressure coefficient, $\frac{p_l - p_0}{q_0}$
D	drag (lb)
M	Mach number
m	mass flow (slugs/sec)
m/m_{max}	ratio of mass flow to maximum mass flow measured at given stream condition
P	total pressure (lb/sq ft absolute)

p	static pressure (lb/sq ft absolute)
q	dynamic pressure, $\frac{\gamma}{2} \rho M^2$ (lb/sq ft)
R	radius (in.)
S	distance (in.)
U	x-component of velocity
u	x-component of perturbation velocity
x	axial distance from cowl lip (in.)
β	ratio of maximum mass flow at given condition to mass flow in free stream having area equal to cowl inlet area
γ	ratio of specific heats

Subscripts:

a	additive drag
c	cowl lip
f	friction drag
l	local
p	pressure

Stations (see fig. 1):

0	free stream
1	diffuser inlet
2	diffuser longeron leading edge
3	combustion-chamber inlet (annular area minus longeron area) (1.034 sq ft)
4	combustion-chamber station 4 (1.394 sq ft)
5	combustion-chamber outlet
6	nozzle outlet

RESULTS AND DISCUSSION

2290

Over-all diffuser pressure recovery. - The over-all diffuser pressure recoveries P_3/P_0 for the three inlets are presented in figure 3 as a function of the mass-flow ratio m/m_{max} for Mach numbers of 1.7, 1.9, and 2.0. At a Mach number of 1.7, only the low cone angle inlet (20-27.4) was unstable in the subcritical flow range investigated. All the inlets exhibited instability in a portion of the subcritical flow range at Mach numbers of 1.9 and 2.0. For the same cone angle, the low mass-flow ratio diffuser (25-31.9) showed a noticeable increase in range of stable subcritical flow compared with the high mass-flow ratio diffuser (25-43.1). The decrease in over-all pressure recovery in the unstable range of mass-flow ratio was more marked, however, with the low mass-flow ratio diffusers. A further comparison between low mass-flow ratio inlets shows the larger cone angle diffusers to have an increased stable subcritical range and a slightly higher pressure recovery than the inlet with the low cone angle.

Diffuser stability. - Total-pressure profiles at the entrance to the inlet, station 1, prior to and during pulsing (fig. 4) provide some insight into the pulsing problem. It is apparent from the profiles that at M_0 of 2.0 a region of low-energy air (separated boundary layer) develops along the cone surface of the low mass-flow ratio inlets prior to pulsing. The adverse pressure gradient across the normal shock is believed to trigger this separation of the cone surface boundary layer so that as the normal shock moves out on the cone the separated low-energy region fills a greater portion of the inlet area and pulsing conditions are approached.

A reduction in M_0 and an increase in cone angle both reduce the adverse pressure gradient across the normal shock. At M_0 of 2.0, the adverse pressure gradient is severe enough to cause separation for both the 20° and 25° inlets. It may be expected, then, that at some M_0 below 2.0 the adverse pressure gradient on the 25° inlet will be mitigated sufficiently to prevent separation. However, the same Mach number will cause separation on the 20° cone. This separation is substantiated at M_0 of 1.7 (see fig. 4) by the total-pressure profiles at the minimum stable subcritical conditions, which indicate for the 25° inlet a reduction in total pressure in the vicinity of the cone surface of but half the value experienced for the 20° inlet. Schlieren photographs for these conditions (fig. 5) offer additional evidence of the flow separation at M_0 of 1.7 occurring only with the 20° inlet, but there is no indication of a vortex sheet. Reference 1 attributes the pulsing of low mass-flow ratio inlets to the vortex sheet separating a high- and low-energy region which originates at

the intersection of the legs of a lambda shock. Also, it specifies that this vortex sheet must enter the inlet near the cowl lip to cause instability. There thus appears to be an additional source of instability for low mass-flow ratio inlets which is dependent only on the development of low-energy air in the region of the center body.

Instability with the high mass-flow ratio inlet, 25-43.1, however, occurred at free-stream Mach numbers of 1.9 and 2.0 when a vortex sheet originating at the intersection of the engine normal and oblique shocks entered just inside the cowl lip; this result agrees well with reference 1. The continued stability of an inlet at a low Mach number (1.7 in this case) may be explained by the weakness of the vortex sheet at low Mach numbers.

In summary, then, by increasing the supersonic spillage around the inlet greater stable subcritical mass-flow regulation is possible. The amount of stable mass-flow regulation possible with a low mass-flow ratio inlet appears to depend on the development and control of the cone boundary layer. Such a control may be accomplished by increased cone angles or by a boundary-layer removal system (references 1 and 5).

The results of both types of inlet appear to be in agreement with reference 6, which relates instability to the slope of the curve of pressure recovery against mass-flow ratio. Prediction of the minimum stable points was not attempted by use of this theory, however, because the rate of change of total-pressure ratio with respect to mass-flow ratio was not well enough defined by the amount of data available for these inlets.

Subsonic diffuser pressure recovery. - The subsonic loss is defined as that measured between stations 1 and 3. The effect of m/m_{\max} on the subsonic diffuser recovery of the three inlets investigated is presented in figure 6. In the range of stable subcritical operation, decreasing the mass-flow ratio generally resulted in improved subsonic diffuser pressure recoveries due to a reduction in flow velocity at the inlet.

At critical mass-flow conditions, the 20° inlet had a stronger shock and a lower Mach number downstream of the normal shock than the 25° inlet. Most of the improvement in over-all pressure recovery gained in using a 25° inlet, however, arises from the reduction in subsonic diffuser losses. A possible explanation is the influence of the strength of the normal shock on the boundary layer. An example of the importance of boundary-layer control on the subsonic losses is presented in reference 7. The geometry of the subsonic flow passages, however, is another factor which could contribute to the large subsonic pressure losses observed with the 20-27.4 inlet.

For some applications of ram jets, it may be desirable to actuate controls with pressures sensed along the cone surface. In order to provide information on the effect of such pressure sensing instrumentation on diffuser performance, data were obtained with two 1/4-inch-diameter total-pressure tubes mounted in a vertical plane on the 20-27.4 inlet approximately 1/2 inch from the cone surface and $3\frac{5}{8}$ inches forward of the cowl lip. The effect of this instrumentation on the over-all pressure recovery at M_0 of 1.7 and 2.0 is shown in figure 7. Not only was the over-all pressure recovery appreciably reduced, but a hysteresis loop was observed during the investigation and is indicated by arrows on the figure.

Drag Evaluation

External-body-drag coefficient. - A comparison of the total external-body-drag coefficients for the three inlets as a function of the mass-flow ratio is shown in figure 8. The curves represent a summation of component drags, whereas the data points are drags determined from force measurements. A reduction in the minimum drag coefficient of approximately 30 percent was measured in changing from the low mass-flow ratio inlets to the high mass-flow ratio inlet over the range of Mach number investigated. The increased stable range of air-flow regulation obtained with the low mass-flow ratio inlets investigated thus comes at the expense of a significant increase in drag. Very little change of drag was observed between inlets 20-27.4 and 25-31.9.

Cowl-pressure-drag coefficient. - The cowl-pressure-drag coefficient $C_{D,p}$ computed from an integration of static pressures along the cowl surface is shown in figure 9 as a function of the mass-flow ratio. For any given inlet the maximum value of $C_{D,p}$ was approximately independent of the stream Mach number in the range from 1.7 to 2.0. A comparison between the 25° half-angle conical inlets shows that the low mass-flow ratio inlet had the lower pressure drag due mainly to less projected frontal area. Also, although its frontal area was less than that of the 25° half-angle high mass-flow ratio inlet, the 20° half-angle low mass-flow ratio inlet caused greater drag.

Representative curves of the pressure distribution over the cowl for the three inlets at critical mass-flow conditions are presented in figure 10 and comparison is made with both conventional linearized theory and linearized theory adjusted to account for the oblique shock configuration as discussed in the appendix. This procedure showed the theoretical and experimental pressure coefficients in close agreement at critical mass flow for the case where the oblique shock originating from the cone fell at or inside the cowl lip (25-43.1 at $M_0 = 2.0$). Agreement was also obtained for the case where the oblique shock falls outside the cowl lip if the streamline next to the outermost entering streamline passes over the cowl lip without an additional deflection of a significant magnitude (25-31.9).

Additive-drag coefficient. - The additive-drag coefficients $C_{D,a}$ computed from a momentum balance between station 0 and 1 are compared (fig. 11) with the theoretical values computed by the method described in reference 3. The experimental values of $C_{D,a}$ for all inlets were predicted with reasonable accuracy by the theory in the stable sub-critical range. The higher additive drag of inlet 25-31.9 tended to offset the higher cowl pressure drag of inlet 20-27.4, so that the total drags of the low mass-flow ratio inlets were approximately equal as previously shown in figure 8.

Friction-drag coefficient. - The friction-drag coefficient $C_{D,f}$ was computed using the method of reference 8, which is based on the change in momentum in the boundary layer along the length of the engine corrected for inlet shock losses. The velocity profiles from which the friction drag was computed varied as the $1/11$ power with distance from the center body and a boundary-layer thickness of $2\frac{1}{8}$ inches was measured at station 5.

Values of friction-drag coefficient of 0.063 ± 0.003 (based on maximum frontal area) were obtained at stable conditions of diffuser operation regardless of the stream Mach number or the mass-flow ratio. The use of a total-temperature variation (see reference 9) in computing friction-drag coefficient increased the friction drag only at M_0 of 2.0, but such refinement was not warranted by the accuracy of the data.

Basing the friction-drag coefficients on wetted area (0.0016) shows good agreement with compressible flat-plate theory of reference 10 (0.00158 at $M_0 = 1.7$). It should be remembered that the measured friction drag was obtained in the tunnel where reflecting shocks are present on the model and may therefore not represent the friction drag to be expected in free flight.

Summation of component drag coefficients. - The external-body-drag coefficients obtained from a summation of the foregoing component drags are shown in figure 8.

Comparing the values of drag coefficient obtained from a summation of component drags with the drag coefficient obtained from the force measurements indicates that the maximum discrepancy for critical flow conditions is approximately 5 percent.

SUMMARY OF RESULTS

The following results were obtained from a study of a 20° and a 25° half-angle low mass-flow ratio and a 25° half-angle high mass-flow ratio

conical supersonic inlet on a 16-inch scale model of a Project Rigel ram-jet engine in the 8- by 6-foot supersonic tunnel:

1. Instability of the low mass-flow ratio inlets was related to the separation of the flow from the cone surface, but the vortex sheet required by the analysis of Ferri and Nucci was not observed. Apparently the development of low-energy air along the cone surface was also a source of diffuser instability.

2. The high mass-flow ratio inlet, which had the least stable subcritical operation, had a minimum drag coefficient approximately 30 percent less than that of the low mass-flow ratio inlets at a stream Mach number of 2.0.

3. The higher additive drag of the 25° low mass-flow ratio inlet tended to offset the higher cowl pressure drag of the 20° inlet, so that the total drags of the two low mass-flow ratio inlets were approximately equal.

4. Experimental values of additive and friction drag agreed reasonably well with theoretically predicted values; for some limited cases the cowl-pressure-drag coefficient at maximum mass-flow ratio for two specific types of shock configuration was predicted theoretically by use of an adjusted linearized potential theory.

Lewis Flight Propulsion Laboratory
National Advisory Committee for Aeronautics
Cleveland, Ohio

APPENDIX

PREDICTION OF COWL EXTERNAL PRESSURE DISTRIBUTION

AT CRITICAL MASS-FLOW RATIOS

With the exception of the band of high pressures near the cowl lip, linearized theory as presented in references 11 and 12 checked the experimental values of pressure coefficient reasonably well for all inlets as shown in figure 10. This band of high pressures, which in fact accounts for the major portion of the pressure drag of the inlets of this report, is due to a constant high slope section of the cowl starting at the sharp edged lip and extending approximately 2 inches rearward.

Case I, Inlet 25-43.1

Two-dimensional shock theory checked the pressures on the outer surface of the cowl lip for the case of inlet 25-43.1 when the undisturbed free-stream air impinged on the cowl at this point. This result suggested the use of a hypothetical free-stream Mach number to adjust the first point of the linearized theory to correspond to the flow obtained by use of two-dimensional shock theory. The hypothetical Mach number can be determined as follows:

Advantage can be taken of the relatively simple form of the following linearized equation (reference 11) for the pressure coefficient of the first point to be determined on the forward portion of a body of revolution:

$$C_p = -\frac{2u}{U} = -\frac{2 \frac{dR}{dx'} \cosh^{-1} \left(\frac{x'}{BR} \right)}{\beta \sqrt{\left(\frac{x'}{BR} \right)^2 - 1} + \frac{dR}{dx'} \cosh^{-1} \left(\frac{x'}{BR} \right)} \quad (1)$$

where $x' = x + BR_C$

Assuming that the linearized form of the pressure coefficient is valid for the case being considered and letting the velocity decrement in the numerator equal the sum of the x-component of velocity decrement across the shock plus the perturbation velocity due to the body contour result in:

$$\begin{aligned}
 C_p'' &= 2 \left(\frac{U_0 - U}{U_0} \right) \\
 &= 2 \left(\frac{U_0 - U_h - u_h}{U_0} \right) \\
 &= 2 \left[1 - \frac{U_h}{U_0} \left(1 + \frac{u_h}{U_h} \right) \right] = 2 \left[1 - \frac{M_h}{M_0} \frac{\left(\frac{a}{a_a} \right)_h}{\left(\frac{a}{a_a} \right)_0} \left(1 + \frac{u_h}{U_h} \right) \right]
 \end{aligned}$$

where the sub h conditions correspond to the flow properties adjusted by using a hypothetical Mach number in equation (1), so that

$$C_p'' = 2 \left[1 - \frac{M_h}{M_0} \frac{\left(\frac{a}{a_a} \right)_h}{\left(\frac{a}{a_a} \right)_0} \left(1 + \frac{u_h}{U_h} \right) \right] = \frac{2 \frac{dR}{dx'} \cosh^{-1} \left(\frac{x'}{B_h R} \right)}{\beta_h \sqrt{\left(\frac{x'}{B_h R} \right)^2 - 1} + \frac{dR}{dx'} \cosh^{-1} \left(\frac{x'}{B_h R} \right)}$$

This equation can be solved by trial and error to find a value of B_h that will satisfy the value of pressure coefficient (C_p'') obtained by two-dimensional shock theory for a given inlet and free-stream Mach number. The value of B_h thus obtained can then be used as a constant for the remainder of the points calculated by use of the hypothetical free-stream Mach number.

$$M_h = \sqrt{B_h^2 + 1}$$

The adjusted linearized theory could thus be used over the high-slope region of the cowl until the point where this curve approached the conventional linearized theory curve, which would then be used to define the pressure distribution over the remaining portion of the cowl. A result of this procedure is shown in figure 10(a), where integration of the resulting theoretical curves agreed within 3 percent of the experimental pressure-drag coefficient shown in figure 9.

Case II, Inlets 20-27.4 and 25-31.9

For the low mass-flow ratio inlets (20-27.4 and 25-31.9), advantage can be taken of the conical nature of the flow field in the region between the oblique shock and station 1 so that a known point can be selected on the outermost entering streamline (determined by use of conical flow

tables given in reference 13) with which to adjust the first point of the linearized theory. The linearized theory can again be adjusted by use of a hypothetical free-stream Mach number, as was done for Case I. Linearized theory based on the hypothetical free-stream Mach number was then used over the outermost entering streamline and over the fore part of the cowl external surface and was found to agree quite well with experimental results for the region of inlet 25-31.9 which could not be previously predicted. Conventional linearized theory based on actual free-stream conditions as presented in reference 11 checked the experimental results for the remainder or low-slope region of the cowl surface.

Poor agreement with experimentation (fig. 10(c)) was obtained, however, for the 40° conical inlet 20-27.4 because of a shock of considerable strength arising from appreciable deflection of the external flow by the cowl lip. The strength of the shock at this position could not be predicted in this case, as it corresponded to a value somewhere between that due to a wedge and that due to a cone.

REFERENCES

1. Ferri, A., and Nucci, L. M.: The Origin of Aerodynamic Instability of Supersonic Inlets at Subcritical Conditions. NACA RM L50K30, 1951.
2. Fisher, R. E.: Controlling the Subcritical Stability of Conical Shock Inlets. Presented at the symposium on the Aerodynamics of Ramjet Supersonic Inlets (Wright-Patterson Air Force Base (Dayton)), Oct. 3rd and 4th, 1950. Marquardt Aircraft Co.
3. Sibulkin, Merwin: Theoretical and Experimental Investigation of Additive Drag. NACA RM E51B13, 1951.
4. Nussdorfer, T., Wilcox, F., and Perchonok, E.: Investigation at Zero Angle of Attack of a 16-Inch Ram-Jet Engine in 8- by 6-Foot Supersonic Wind Tunnel. NACA RM E50LC4, 1951.
5. Obery, Leonard J., Englert, Gerald W., and Nussdorfer, Theodore J.: Pressure Recovery, Drag, and Subcritical Stability Characteristics of Conical Supersonic Diffusers with Boundary-Layer Removal. NACA RM E51H29, 1952.
6. Sterbentz, William H., and Evvard, John C.: Criteria for Prediction and Control of Ram-Jet Flow Pulsations. NACA RM E51C27, 1951.
7. Goelzer, H. Fred, and Cortright, Edgar M., Jr.: Investigation at Mach Number 1.88 of Half of a Conical-Spike Diffuser Mounted as a Side Inlet with Boundary-Layer Control. NACA RM E51G06, 1951.

8. Luidens, Roger W., and Madden, Robert T.: Interpretation of Boundary-Layer Pressure-Rake Data in Flow with a Detached Shock. NACA RM E50I29a, 1950.
9. Tucker, Maurice, and Maslen, Stephen H.: Turbulent Boundary-Layer Temperature Recovery Factors in Two-Dimensional Supersonic Flow. NACA TN 2296, 1951.
10. de Kármán, Th.: The Problem of Resistance in Compressible Fluids. Quinto Convegno "Volta", Reale Accademia d'Italia (Roma), Sett. 30-Ott. 6, 1935, pp. 3-57.
11. Brown, Clinton E., and Parker, Hermon M.: A Method for the Calculation of External Lift, Moment, and Pressure Drag of Slender Open-Nose Bodies of Revolution at Supersonic Speeds. NACA Rep. 808, 1945. (Formerly NACA ACR L5L29).
12. Moore, Franklin: Linearized Supersonic Axially Symmetric Flow about Open-Nosed Bodies Obtained by Use of Stream Function. NACA TN 2116, 1950.
13. Anon.: Tables of Supersonic Flow Around Cones. Tech. Rep. No. 1, Dept. Elec. Eng., M. I. T. (Cambridge), 1947.

TABLE I - TABLE OF COORDINATES FOR AFTERBODY
OF 16-INCH RAM JET

Distance from inlet attachment station (in.)	Inner body diameter (in.)	Outer body outside diameter (in.)
0	11.70	15.64
24.75	11.70	16.50
40.00	11.13	Constant
68.39	10.08	to
74.28	9.78	↓
81.14	8.96	16.500
86.82	7.75	Straight
100.89	Conical to	taper to
101.61	3.43	16.250
106.61		Constant to
159.98		16.250

NACA

2290

TABLE II - COORDINATES FOR VARIOUS INLET CONTOURS

Distance from core apex (in.)	Diameters, in.		
	Inner body	Outer body	
		Inner surface	Outer surface
Inlet, 20-27.4			
0	0		
11.437 ^a	Conical	11.81	11.83
12.187	to	12.24	12.49
12.937	↓	12.68	13.11
15.100	10.99	13.89	14.39
16.054	11.51	14.21	14.71
17.103	11.70	14.32	14.82
18.437	Constant	14.40	14.90
	diam.	Straight	Taper →
31.66	11.70	15.14	15.64
Inlet, 25-31.9			
0	0		
	Conical to	12.15	12.17
9.78	9.120	12.39	12.52
10.24	9.540	12.780	13.02
10.88	10.020	13.200	13.72
11.88	10.560	13.500	14.01
12.88	10.960	13.880	14.39
14.88	11.420	13.980	14.49
15.88			
19.663	11.700	Straight to	Taper to
	Constant	↓	↓
	diam. to		
30.022	11.700	15.140	15.640
Inlet, 25-43.1			
0	0		
5.000 ^a	Conical to	9.360	9.380
5.820	5.428		10.000
6.880	6.310	10.284	10.784
8.880	7.590	11.114	11.614
10.730	8.310		
10.880		11.628	12.128
12.880	8.840	12.054	12.554
14.880	9.260	Straight	Straight
16.880	9.660	taper	taper
19.660 ^b	10.200	to	to
22.880	10.756	↓	↓
24.308	10.970		
26.880	11.860		
30.022	11.700	15.140	15.640

^a Station 1.^b Station 2.

NACA

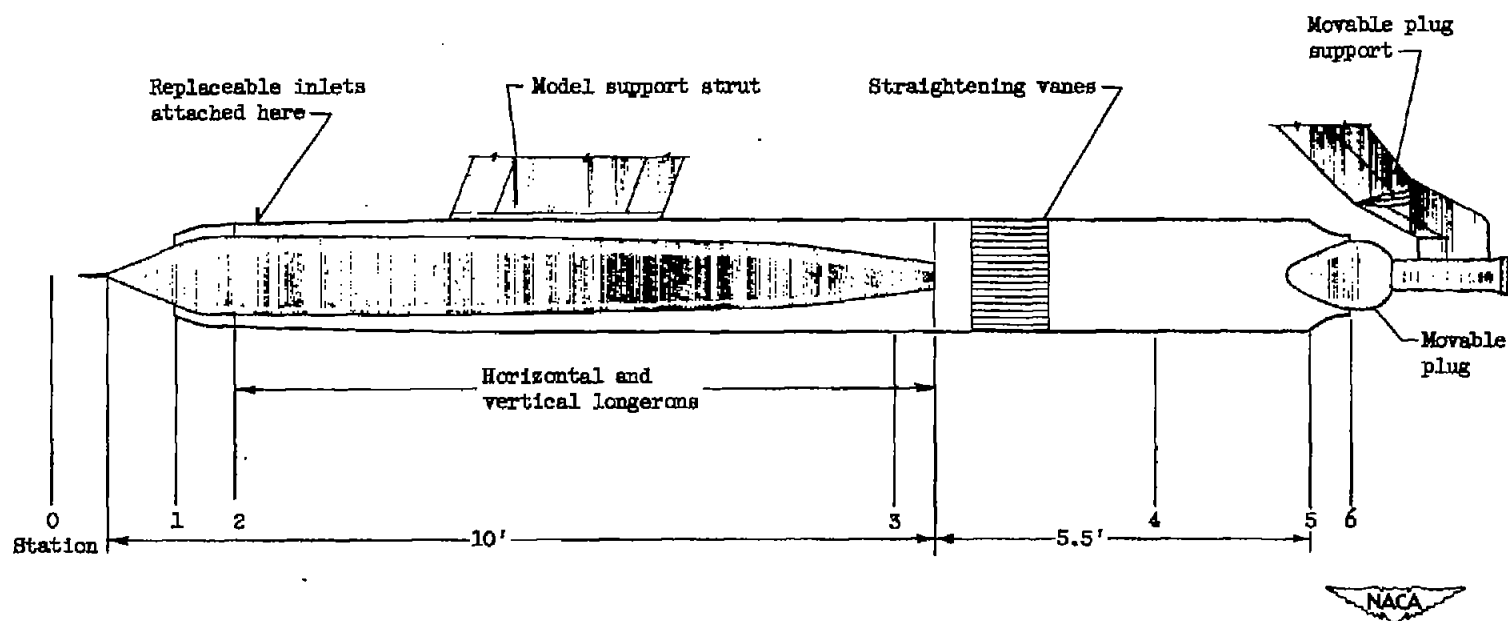


Figure 1. - Diagrammatic sketch of 16-inch ram jet.

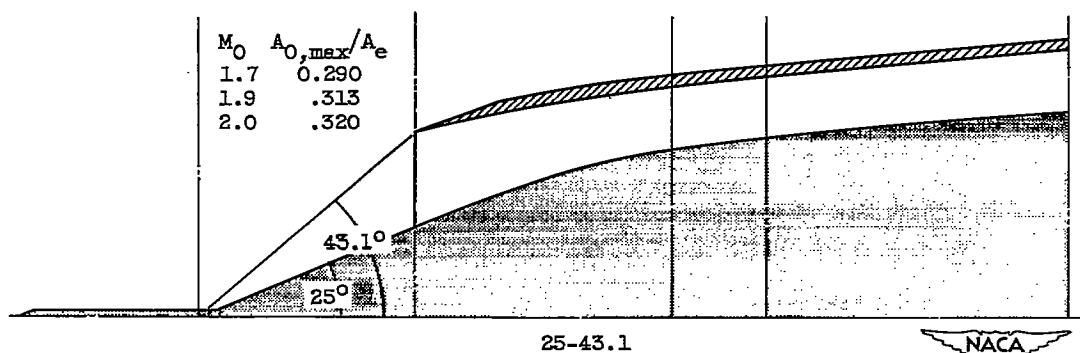
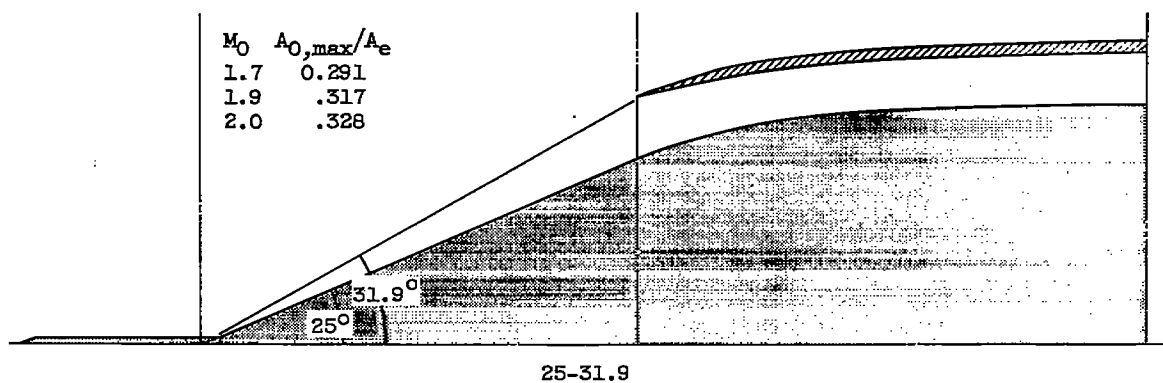
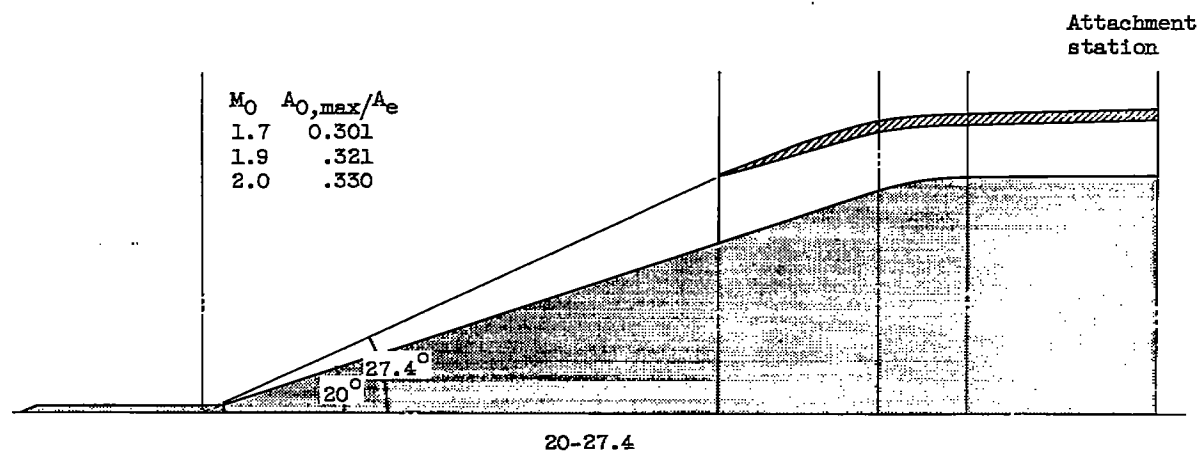


Figure 2. - Geometric comparison of inlets. $A_{0,max}/A_e$ is equal to maximum free-stream tube area divided by maximum combustion-chamber area.

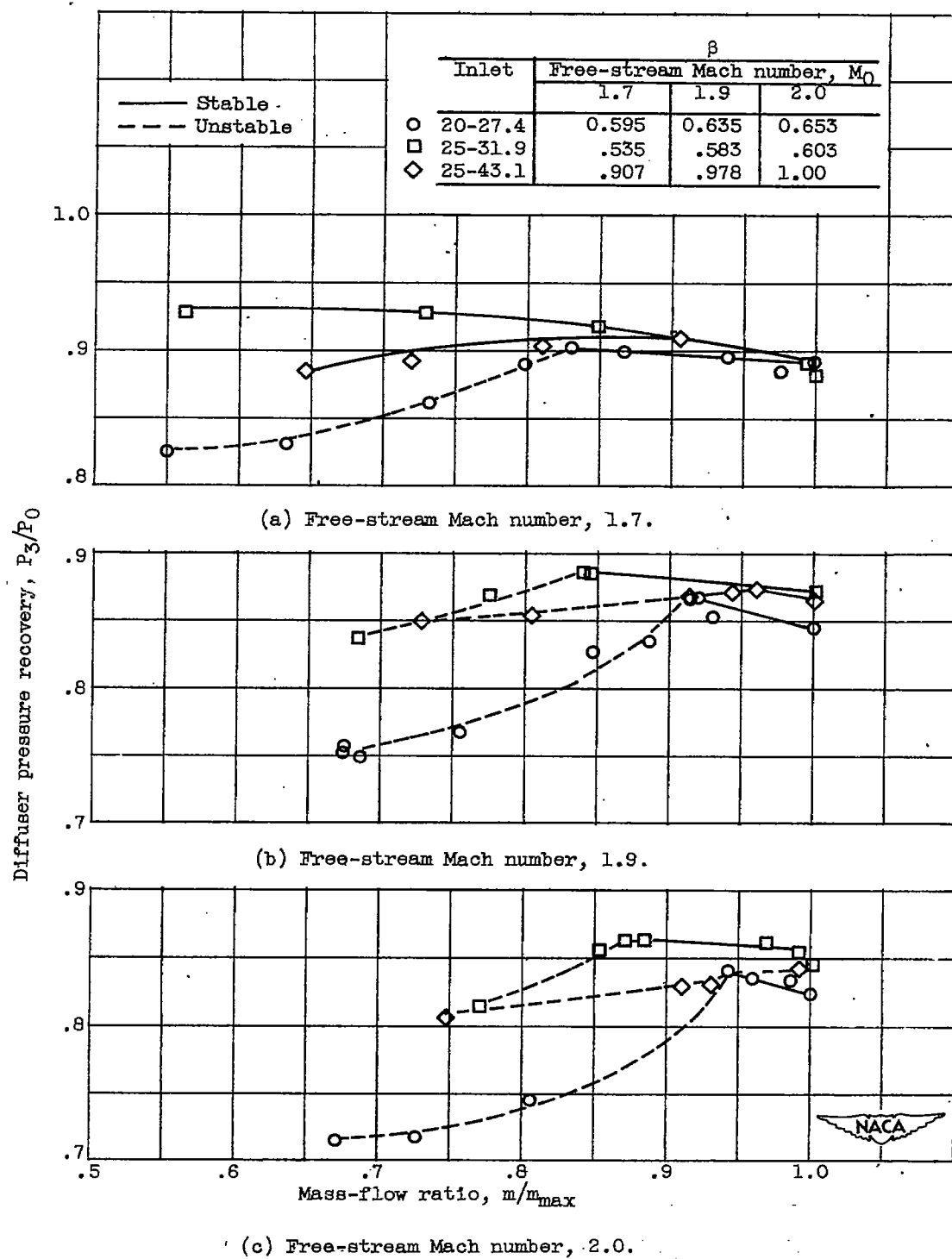
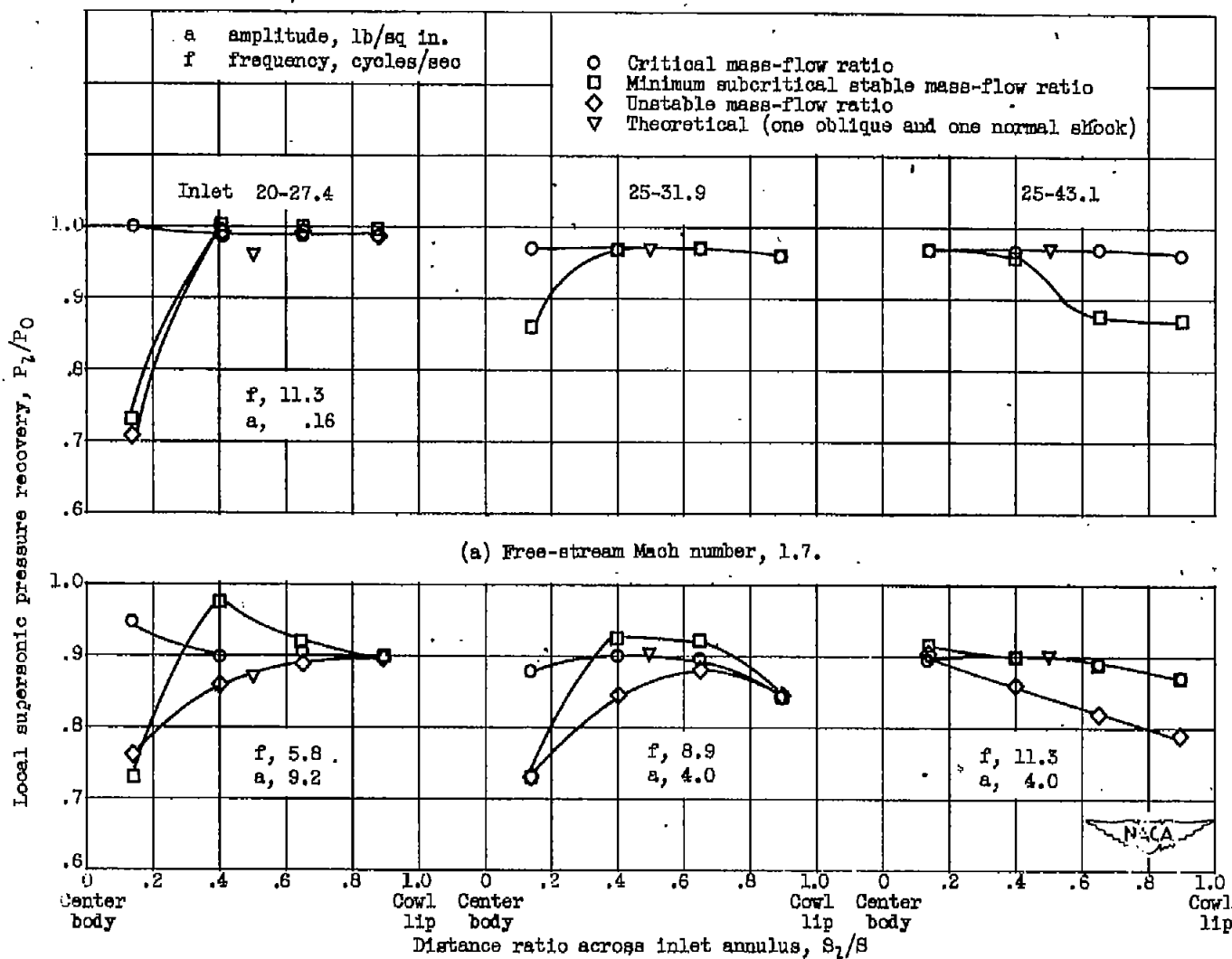
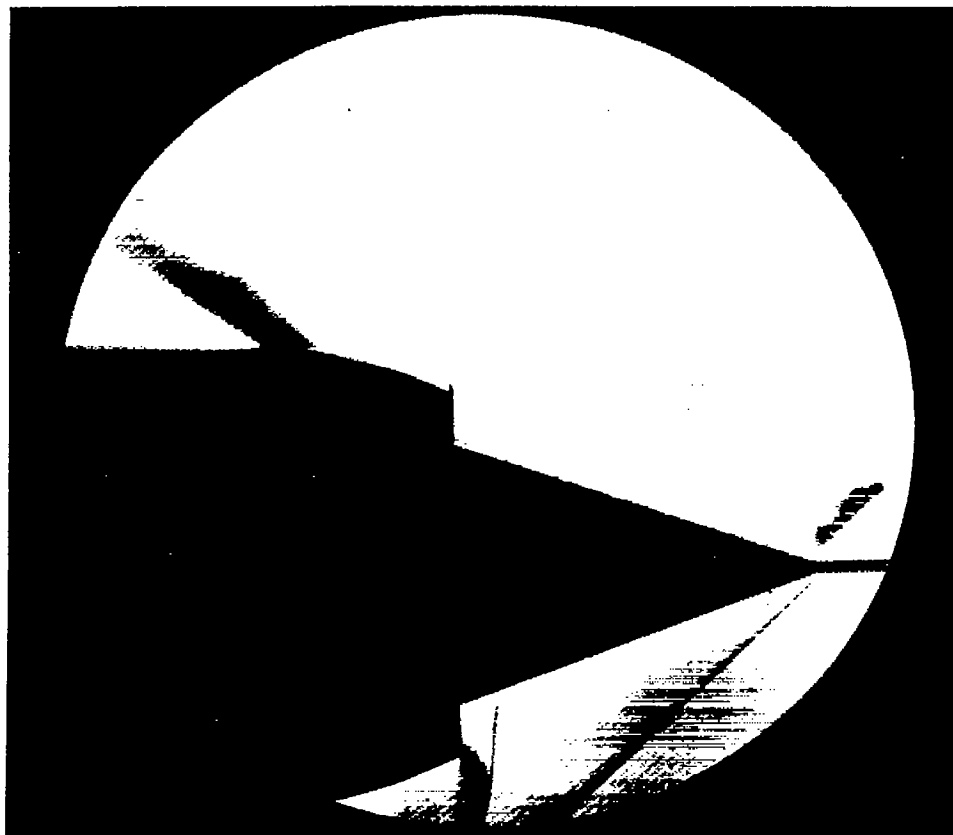


Figure 3. - Variation of diffuser pressure recovery with mass-flow ratio.



(b) Free-stream Mach number, 2.0.

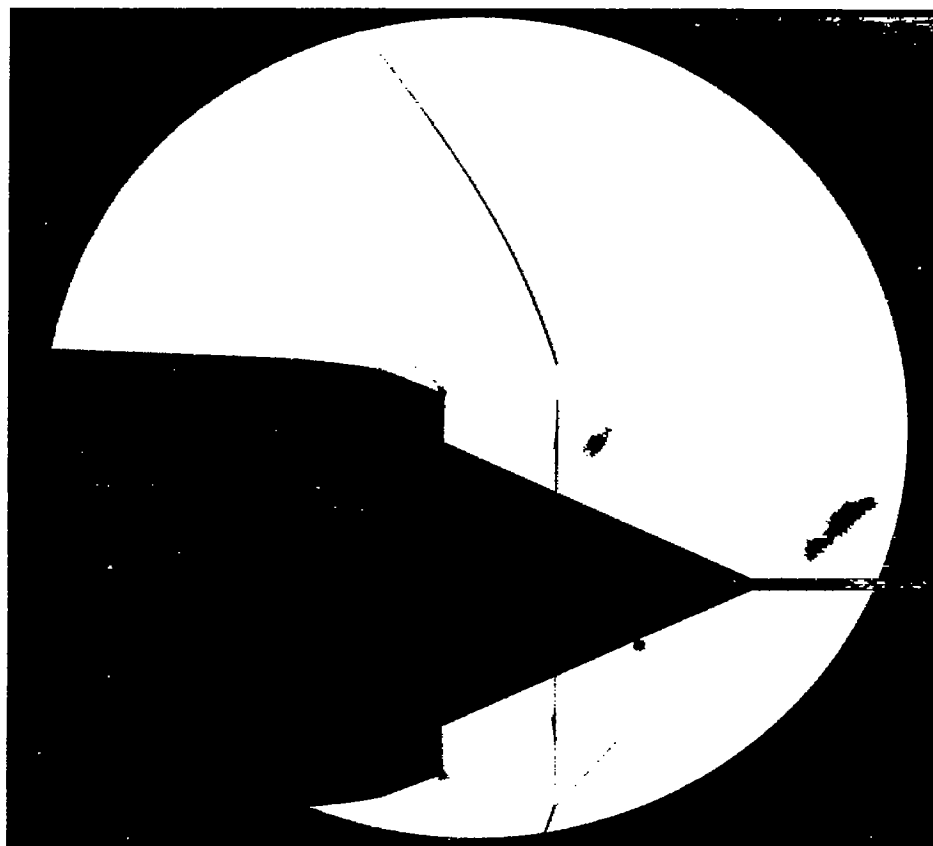
Figure 4. - Total-pressure profiles at station 1 for stream Mach numbers of 1.7 and 2.0.



NACA
C 28034

(a) 20° half-angle low mass-flow ratio inlet. Mass-flow ratio, 0.830 (minimum subcritical stable point).

Figure 5. - Schlieren photographs of three inlets at stream Mach number 1.7.

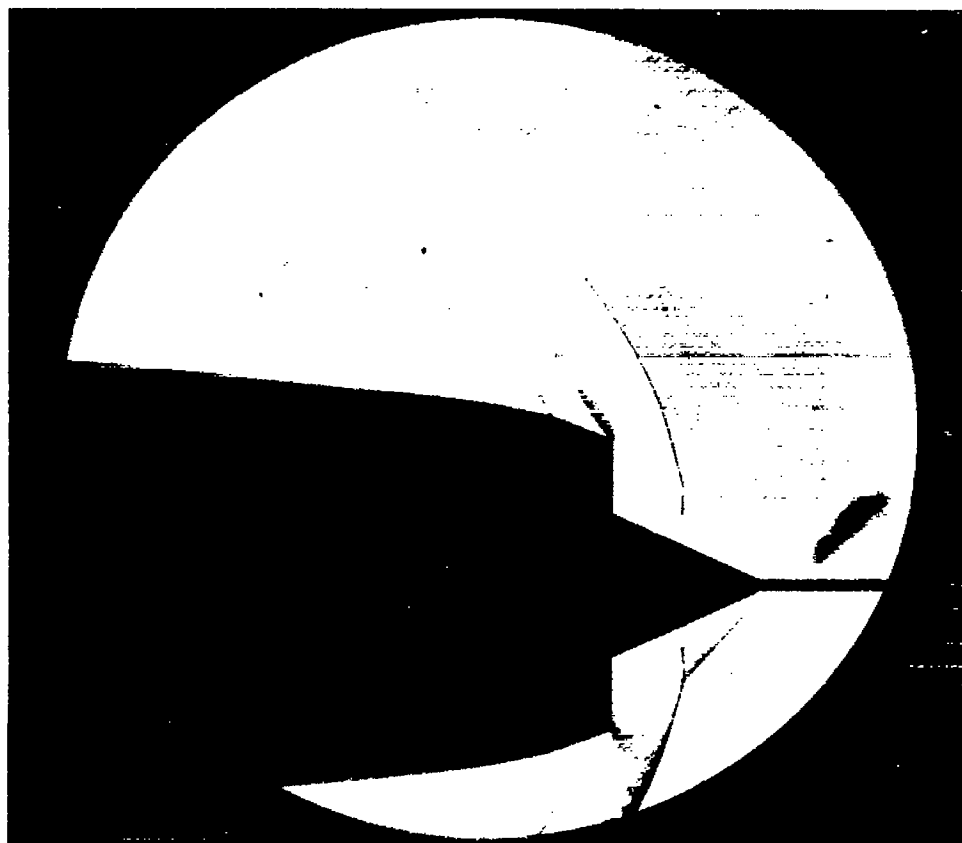


NACA

C-28033

(b) 25° half-angle low mass-flow ratio inlet. Mass-flow ratio, 0.563.

Figure 5. - Continued. Schlieren photographs of three inlets at stream Mach number 1.7.



NACA

E51H27

(c) 25° half-angle high mass-flow ratio inlet. Mass-flow ratio, 0.645.
Figure 5. - Concluded. Schlieren photographs of three inlets at stream Mach number 1.7.

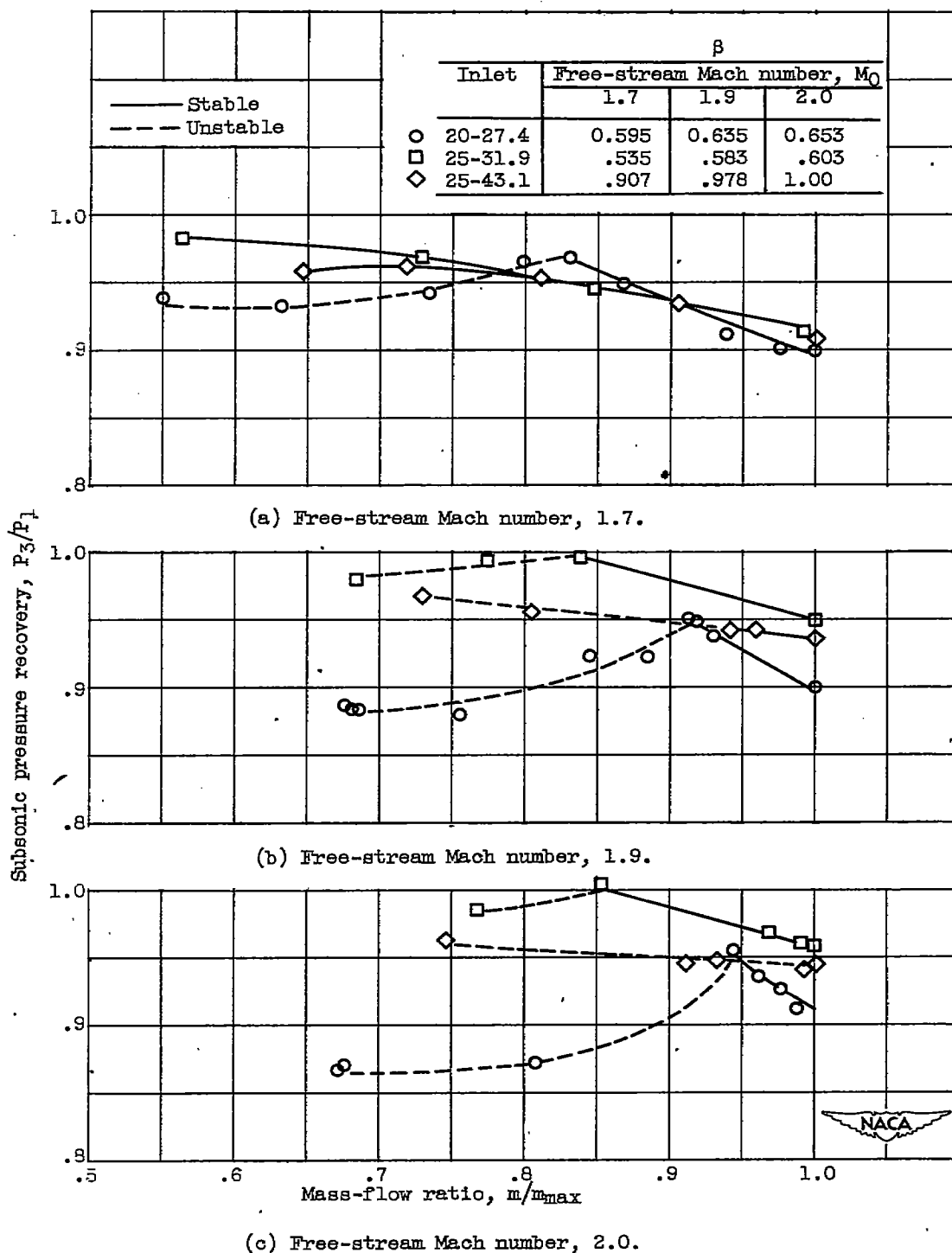


Figure 6. - Variation of subsonic pressure recovery with mass-flow ratio.

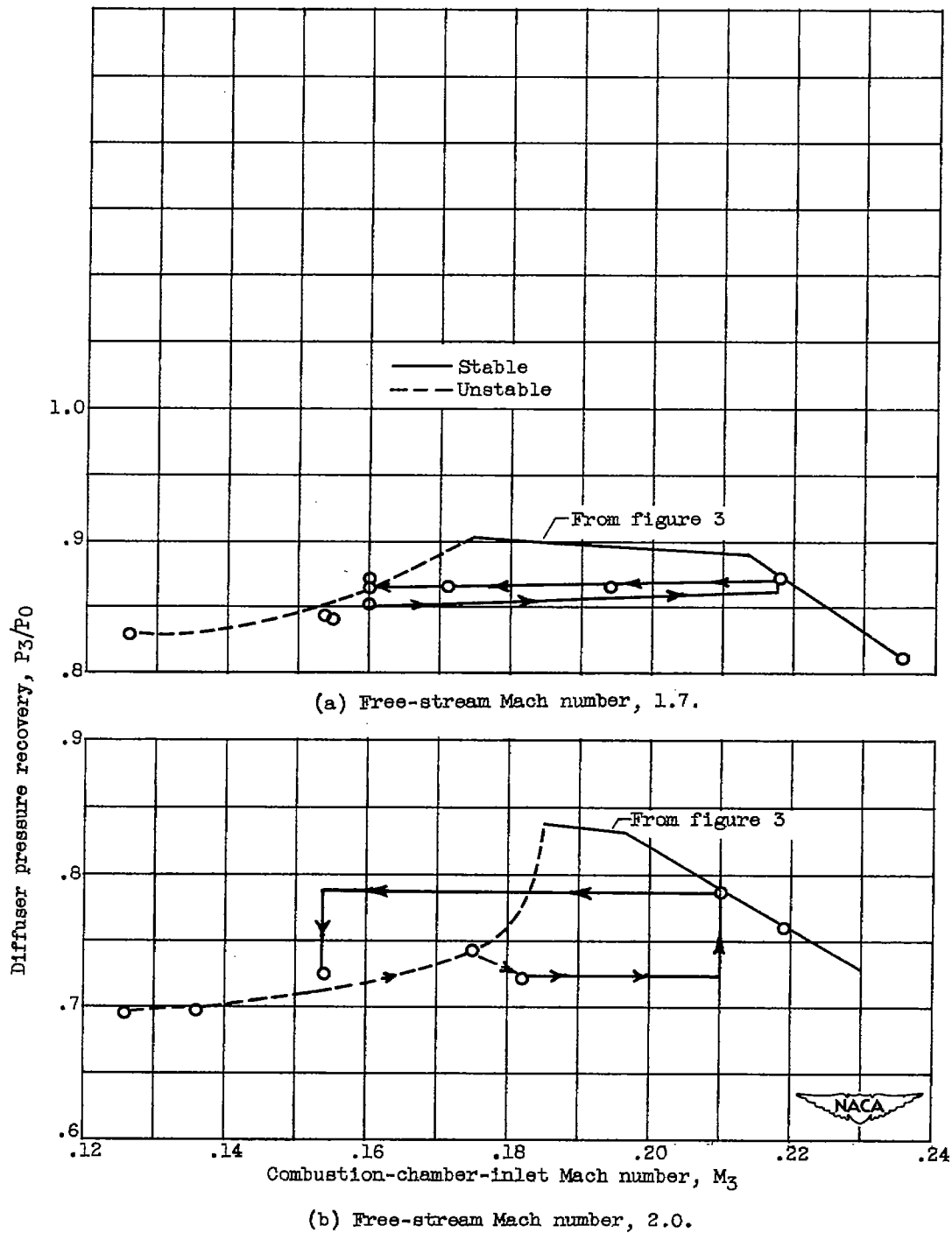
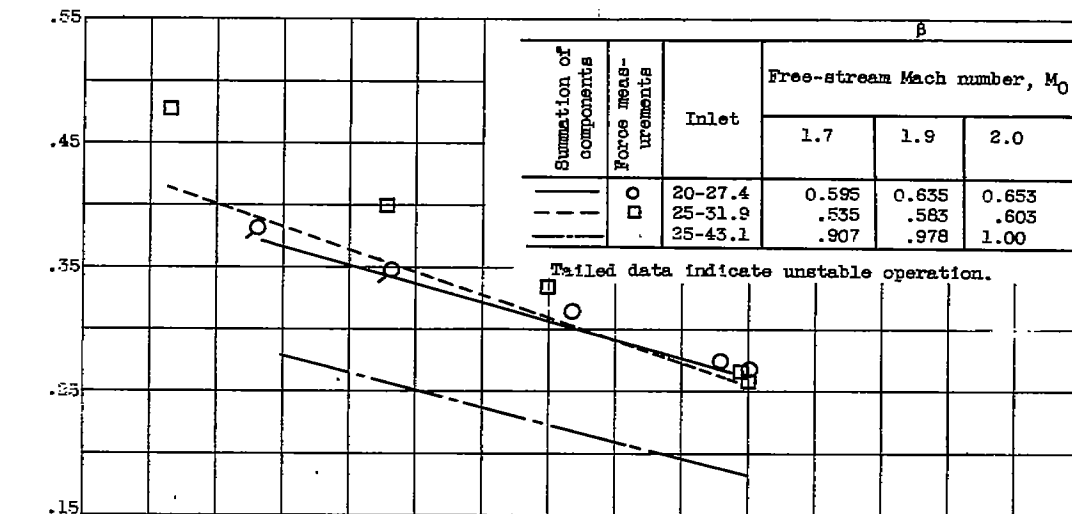
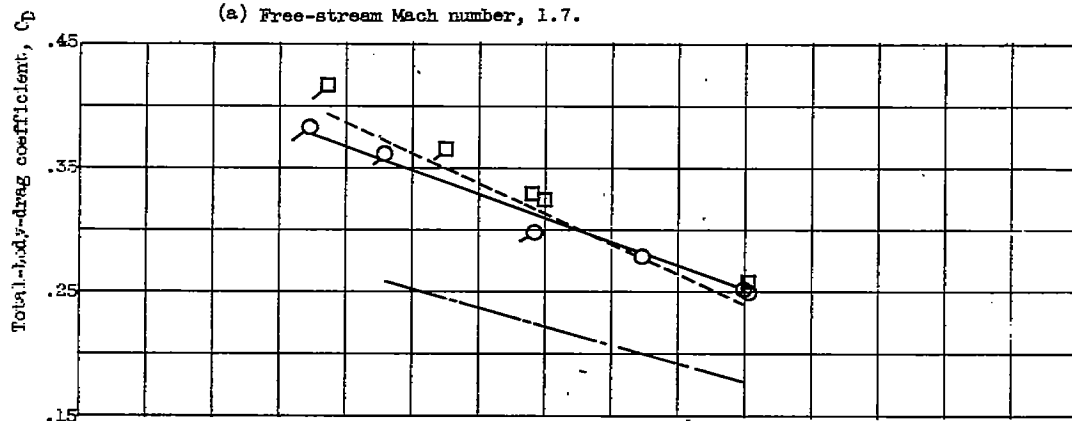


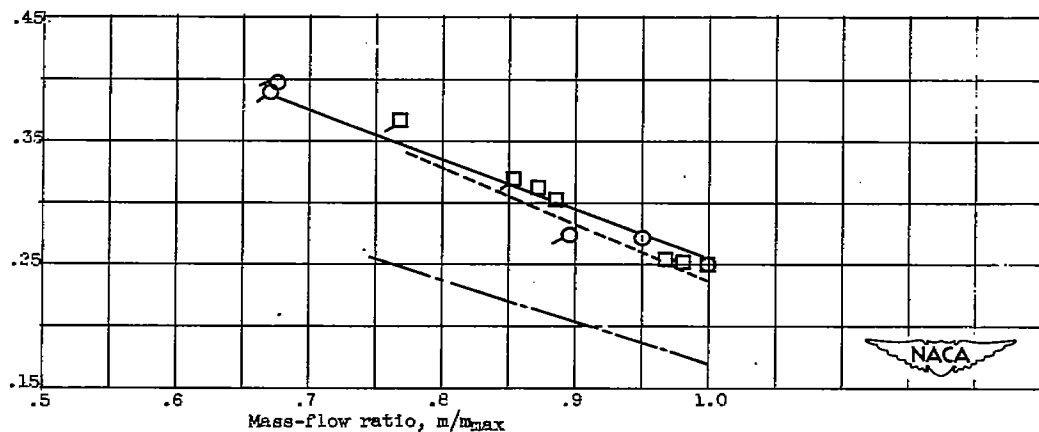
Figure 7. - Effect of instrumentation on diffuser pressure recovery.



(a) Free-stream Mach number, 1.7.

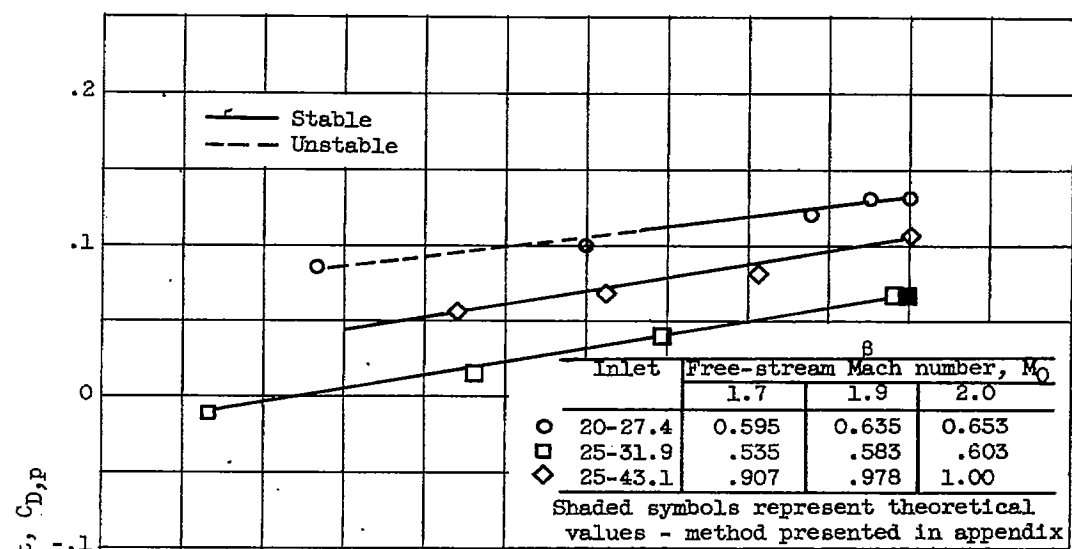


(b) Free-stream Mach number, 1.9.

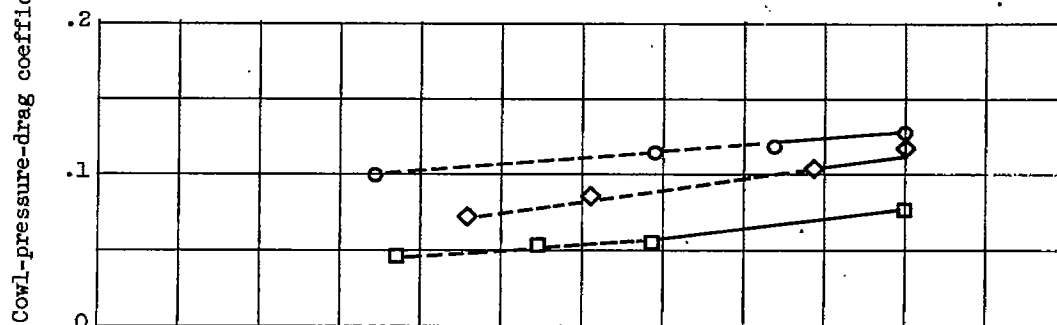


(c) Free-stream Mach number, 2.0.

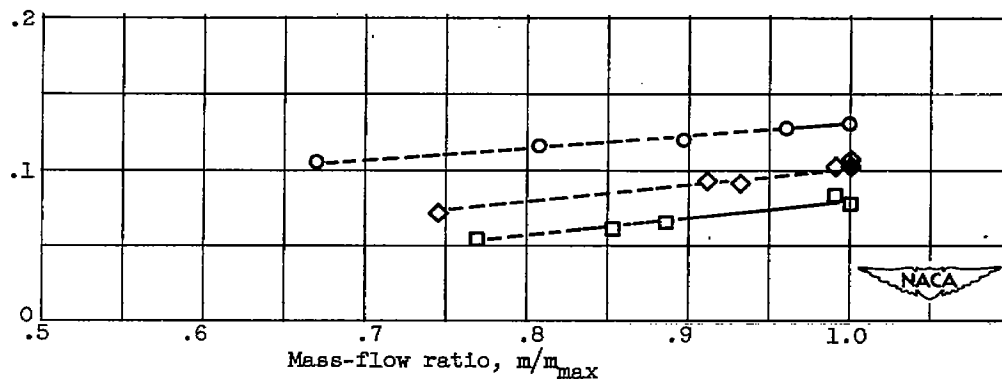
Figure 8. - Variation of total-body-drag coefficient with mass-flow ratio.



(a) Free-stream Mach number, 1.7.

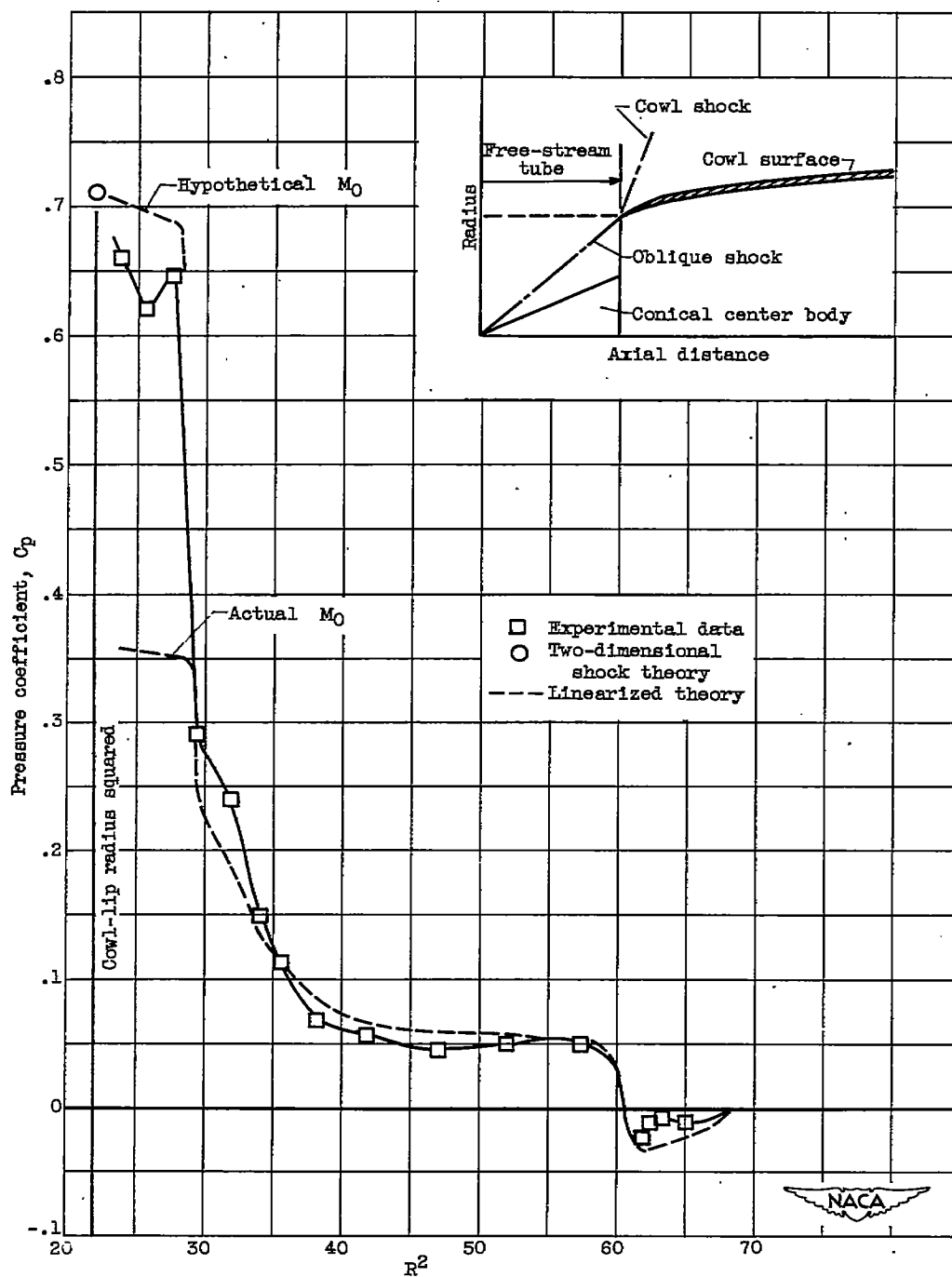


(b) Free-stream Mach number, 1.9.



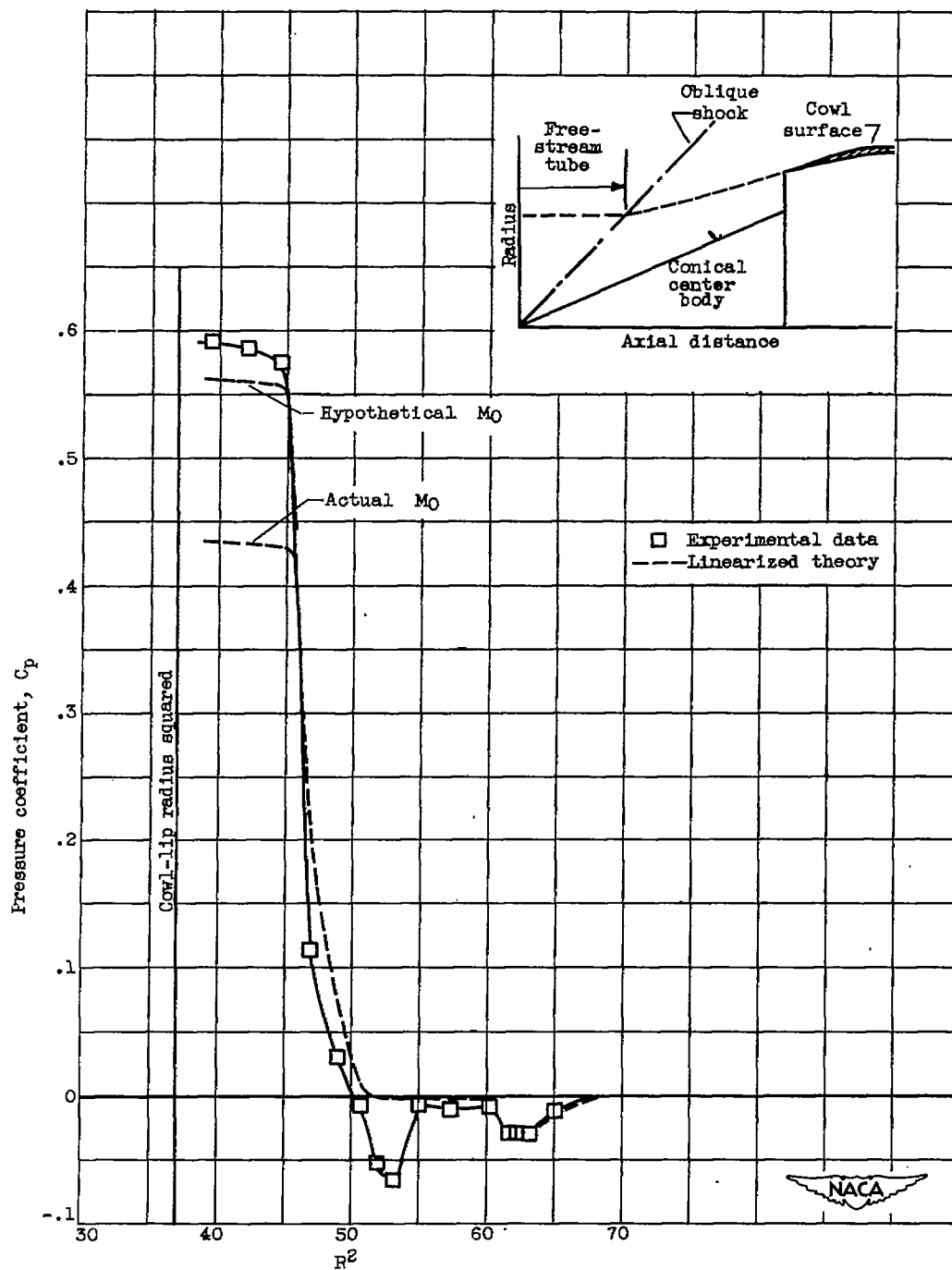
(c) Free-stream Mach number, 2.0.

Figure 9. - Variation of cowl-pressure-drag coefficient with mass-flow ratio.



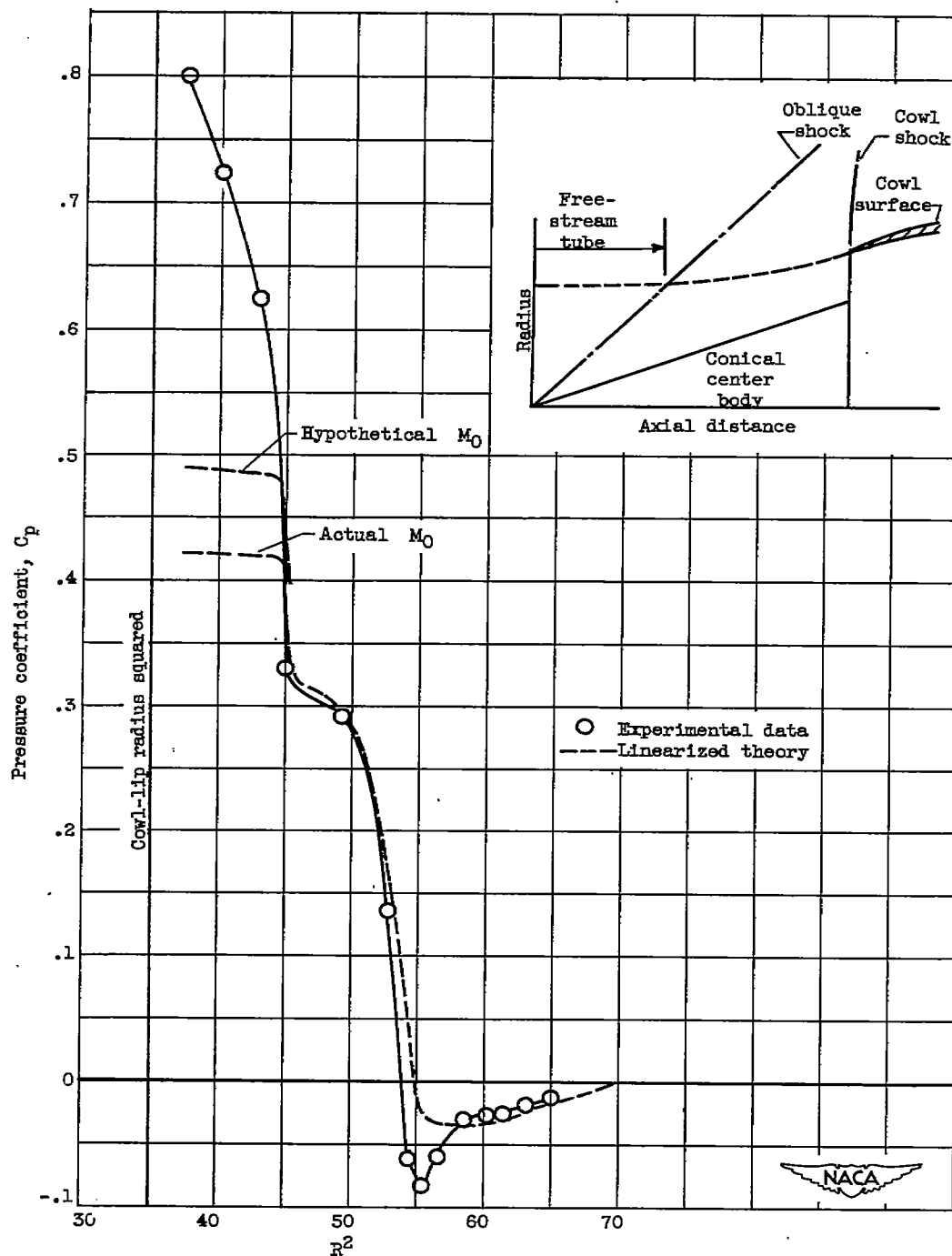
(a) Inlet, 25-43.1; free-stream Mach number, 2.0.

Figure 10. - Pressure distribution over external cowl surface at critical mass-flow ratio.



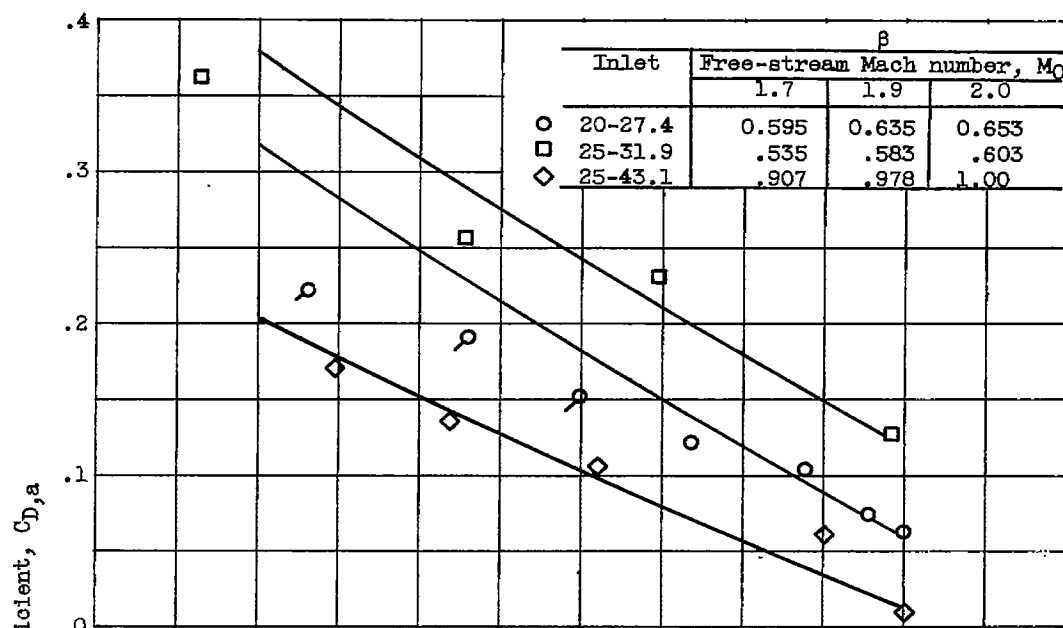
(b) Inlet, 25-31.9; free-stream Mach number, 1.7.

Figure 10. - Continued. Pressure distribution over external cowl surface at critical mass-flow ratio.

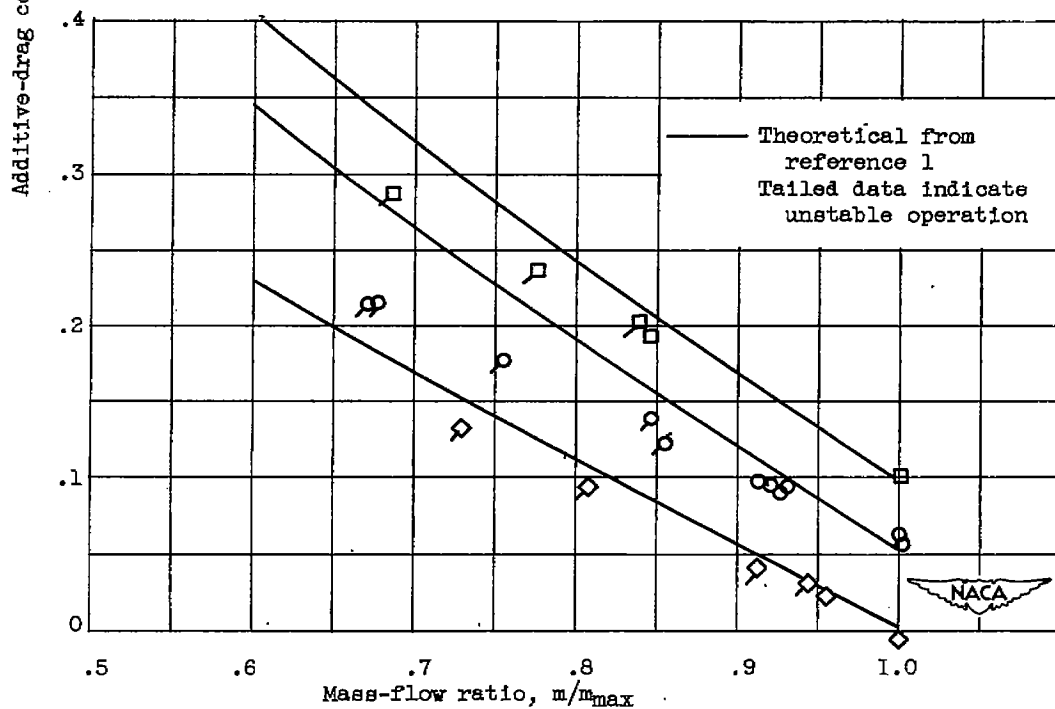


(c) Inlet, 20-27.4; free-stream Mach number, 1.7.

Figure 10. -- Concluded. Pressure distribution over external cowl surface at critical mass-flow ratio.

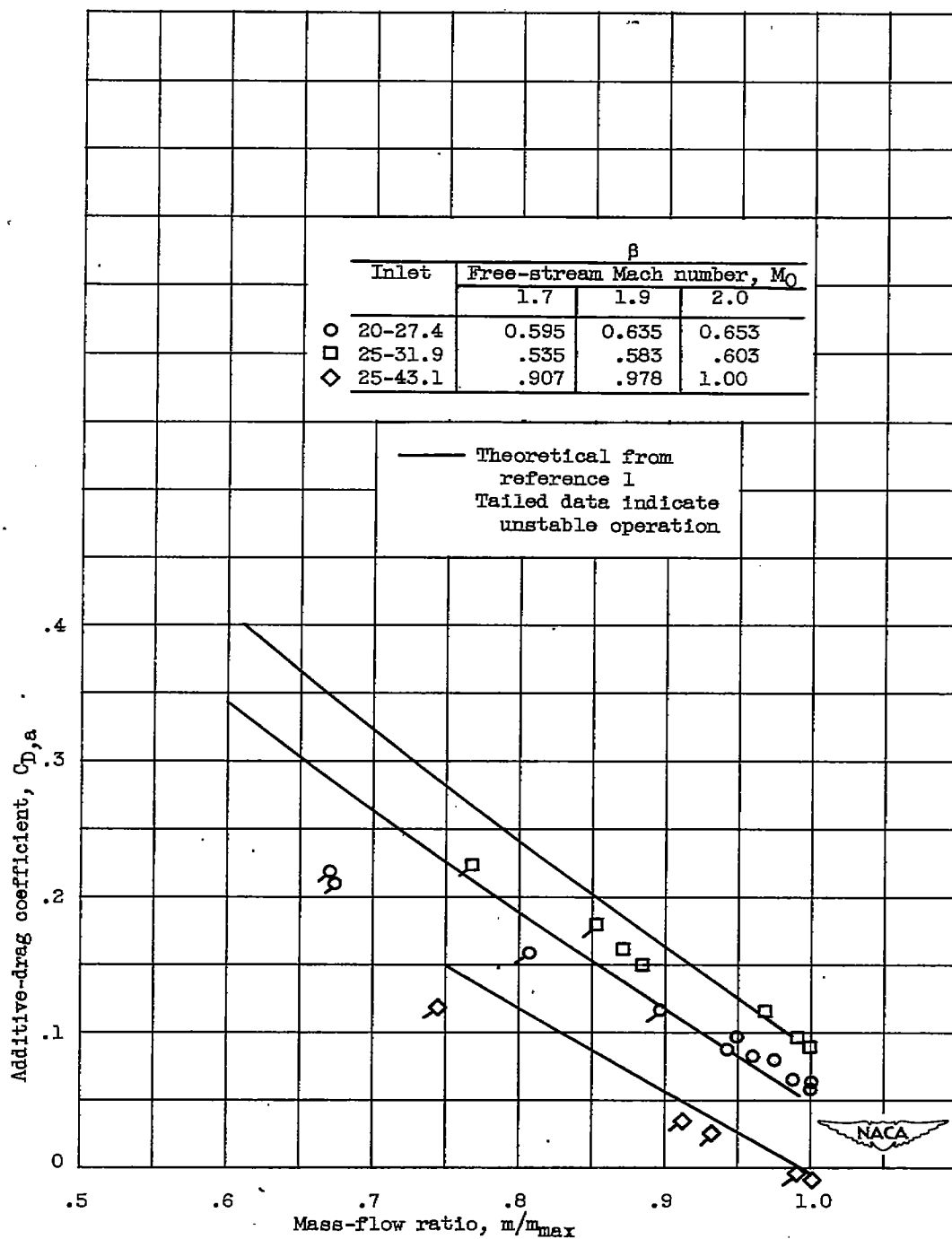


(a) Free-stream Mach number, 1.7.



(b) Free-stream Mach number, 1.9.

Figure 11. - Variation of additive-drag coefficient with mass-flow ratio.



(c) Free-stream Mach number, 2.0.

Figure 11. - Concluded. Variation of additive-drag coefficient with mass-flow ratio.

